arXiv:2409.08431v1 [physics.atom-ph] 12 Sep 2024

Confinement-induced field-linked states of ultracold polar molecules

Reuben R. W. Wang[1, 2, 3] and John L. Bohn[3]

[1] *ITAMP, Center for Astrophysics | Harvard & Smithsonian, Cambridge, Massachusetts 02138, USA*
[2] *Department of Physics, Harvard University, Cambridge, Massachusetts 02138, USA*
[3] *JILA, NIST, and Department of Physics, University of Colorado, Boulder, Colorado 80309, USA*

(Dated: September 16, 2024)

We predict the existence of stable bound states between pairs of ultracold diatomic molecules with the aid of a static electric field and 1D harmonic confinement. We focus on collisions of NaK-NaK identical fermions, for which we find that currently achievable experimental parameters allow the observation of these confinement-induced field-linked bound states as scattering resonances. The bound state is highly stable with lifetimes estimated to be tens of seconds long. With the diatomic molecules bound at distances a fraction of the dipolar length scale, these complexes allow for explorations of polyatomic chemistry and Fermi gas superfluid pairing.

Introduction. Key to the exploration and applications of ultracold molecular gases is the ability to control what these molecules are doing. One form of control manipulates the center-of-mass motion of the molecules, for example with optical lattices [1–4] that lend to the design of molecular ensembles for exploring many-body [5] and low-dimensional [6–9] physics. Trapping can also drastically alter the scattering properties of ultracold colliders through so-called confinement-induced resonances (CIR): dramatic variations in the scattering cross section at certain collision parameters due to external confinement [10, 11]. These resonances require the influence of excited trap states to significantly modify the native two-particle interactions, having seen extensive study in both theoretical [12–18] and experimental [19–22] settings with atomic platforms.

A second form of control exploits the innate dipole-dipole interaction between pairs of interacting molecules, by means of applied static electric or microwave fields. These fields can be used to engineer the very shape of two-molecule interaction potentials for achieving desired Hamiltonians [23–26] and scattering outcomes [27–38]. Varying the strength and properties of these fields have been used to realize collisional shielding to mitigate inelastic collisions [39–48] and to produce near-threshold resonances known as field-linked states [49]. The latter of these cases has led to the formation of long-lived tetratomic complexes [50] by electroassociation [51], which assembles these tetramers by ramping a parameter of the microwave field. Resonant states of this sort are valuable as a way to engineer interactions that may lead to superfluidity [52–54], or else serve as a "launch-pad" from which to initiate a chemical reaction under completely controlled circumstances.

In this Letter, we propose a combination of the two kinds of control – a 1D optical lattice and precise electric field tuning – to produce a different kind of tetramer state. Because their physics arises from confinement effects in the trap as well as linking due to dipoles, we dub these states "confinement-induced field-linked" states (CIFLs). They have distinct advantages over field-linked states observed in unconfined, 3D geometries [49, 50], inasmuch as they are smaller in extent relative to the scale of dipolar interactions, and stabler against decay, making them prominent candidates for further applications.

Formulation. To isolate the key physical aspects of relevance, we consider ultracold, spinless polar molecules prepared in their absolute electronic-vibrational ground state $X^1\Sigma(\nu = 0)$. Harmonic confinement is applied along the z-axis with trapping angular frequency ω_z, along with a strong external electric field $\boldsymbol{\mathcal{E}}$, aligned in the z direction, which induces a lab-frame dipole moment, d and long-range dipole-dipole interaction (DDI) between molecules. With near Kelvin-scale rotational splittings, the molecules can be assumed as strictly polarized along the field axis, rendering the total intermolecular potential in the relative coordinates of the two molecules

$$V_{\text{total}}(\rho, z) = V_{\text{trap}}(z) + V_{\text{int}}(\rho, z), \tag{1}$$

respectively denoting a trap and molecular interaction potential:

$$V_{\text{trap}}(z) = \frac{1}{2}\mu\omega_z^2 z^2, \tag{2a}$$

$$V_{\text{int}}(\rho, z) = V_{\text{DDI}}(\rho, z) + V_{\text{vdW}}(\rho, z) = \frac{d^2}{4\pi\epsilon_0}\frac{1 - 3\cos^2\theta}{(\rho^2 + z^2)^{3/2}} - \frac{C_6}{(\rho^2 + z^2)^3}, \tag{2b}$$

where μ is the reduced mass, C_6 the van der Waals coefficient, ϵ_0 the electric constant and $\cos^2\theta = z^2(\rho^2 + z^2)^{-1}$.

For concreteness, we focus on ^{23}Na^{40}K molecules as a representative example. These molecules have a molecular frame dipole moment of $d_0 = 2.72$ [54] and van der Waals coefficient of $C_6 = 561070$ a.u. [55]. As the two molecules approach radially along ρ, tight vertical confinement will only allow restricted molecular motion in z, resulting in repulsive interactions and a collisionally stable gas useful for explorations of 2D physics [9, 56]. However, if the molecules were more weakly confined to allow larger vertical motion at small ρ, the anisotropic DDI potential can become attractive and usher the molecules

into the short-range associated with lossy dynamics. The scenarios described above are encompassed by a plot of $V_{\rm total}(\rho, z)$ in Fig. 1 (parameters in figure caption), showing the regions of repulsion and attraction as a function of ρ and z [57].

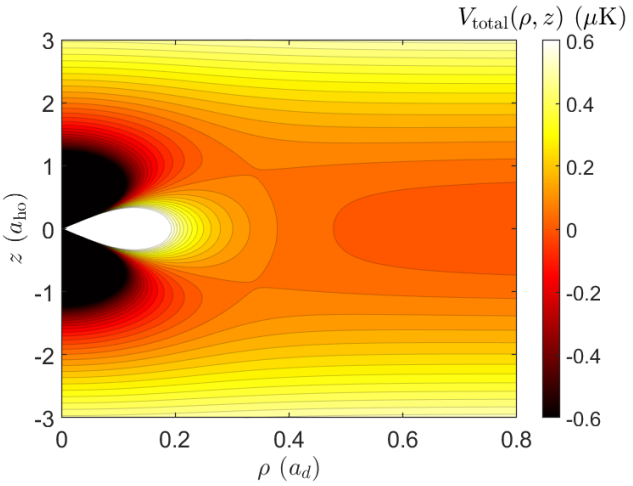

FIG. 1. Contour plot of the potential energy surface between two $Na^{23}K^{40}$ molecules subject to harmonic confinement along z with frequency $\omega_z = 2\pi \times 2.5$ kHz and an applied electric field of $\mathcal{E} = 15$ kV/cm. The vertical and horizontal plot axes are given in units of harmonic oscillator length $a_{\rm ho}$ and dipole length a_d respectively. The colorbar saturates at $|V_{\rm total}| = 600$ nK for clarity of presentation.

Numerical solutions to the Schrödinger equation are obtained by expanding the wavefunction into a basis of harmonic oscillator states $\varphi_n(z)$, azimuthal harmonics $e^{im\phi}/\sqrt{2\pi}$ and radial wavefunctions $u_n^m(\rho)/\sqrt{\rho}$ [58]

$$\frac{1}{2}\delta_{n',n}\left(\frac{\partial^2}{\partial\tilde{\rho}^2} + \tilde{k}^2\right) u_n^m(\tilde{\rho}) = \tilde{U}^m_{n',n}(\tilde{\rho}) u_n^m(\tilde{\rho}), \qquad (3)$$

with wavenumber $k^2 = 2\mu E/\hbar^2$ and effective interaction matrix elements

$$\tilde{U}^m_{n',n}(\tilde{\rho}) = \delta_{n',n}\left(\frac{m^2 - 1/4}{2\tilde{\rho}^2} + \frac{n}{\tilde{a}_{\rm ho}^2}\right) + \tilde{V}^m_{n',n}(\tilde{\rho}), \qquad (4a)$$

$$V^m_{n',n}(\rho) = \int \varphi^*_{n'}(z) V_{\rm int}(\rho, z) \varphi_n(z) dz. \qquad (4b)$$

Above, $a_d = \mu d^2/(4\pi\epsilon_0\hbar^2)$, $a_{\rm ho} = \sqrt{\hbar/(\mu\omega_z)}$ and $a_{\rm vdW} = (\mu C_6/\hbar^2)^{1/4}$ are the dipole, harmonic oscillator and van der Waals lengths respectively. Tildes denote dimensionless quantities as normalized by natural dipole units μ, a_d and the dipole energy $E_{\rm dd} = \hbar^2/(\mu a_d^2)$ [59].

The molecules are assumed prepared in the lowest harmonic oscillator $n = 0$ state, where parity symmetry restricts couplings of $n = 0$ to only even-n channels via DDI during a collision. Fermi symmetry then enforces the molecular-pair wave function to be antisymmetric, only allowing odd partial waves m to be involved in the scattering process.

Confinement-induced field-linked states. To illustrate the origin of the CIFL states, we consider a specific example where the NaK molecules are exposed to an electric field of $\mathcal{E} = 15$ kV/cm and a vertical harmonic trap with $\omega_z = 2\pi \times 2.5$ kHz. These parameters, shown achievable in recent molecular experiments [9], result in the adiabatic curves for the lowest $m = 1$ partial wave plotted in Fig. 2 (solid black curves). The lowest of these curves, denoted $U_{\rm ad}(\rho)$, is the one that holds the CIFLs (red line in left figure inset) [60]. The shape of this curve depends on the different physical circumstances that dominate at different length scales. The largest length scale is the dipole length a_d ($= 3.55 \times 10^4 a_0$ in the example shown), significantly larger than the harmonic oscillator length $a_{\rm ho} = 6.77 \times 10^3 a_0$. Thus when the molecules are far apart, on the scale of $\rho \geq a_d$, their relative coordinate is confined near $z = 0$ and they experience a repulsive interaction [58, 61, 62], as can be seen from the large-ρ, $z \approx 0$ region of Fig. 1. As the molecules get much closer together, and in particular when $\rho < a_{\rm ho}$, for example $\rho \approx 0.1 a_d$, the harmonic oscillator confinement plays a different role. The adiabatic wave function is a solution to the z-dependent Schrödinger equation at fixed ρ. And for $\rho \approx 0.1 a_d$, one sees from Fig. 1 that this solution involves a deep potential energy at displacements away from $z = 0$, in which configuration the dipoles are mostly attractive. The adiabat $U_{\rm ad}(\rho)$ becomes attractive in this range of ρ.

At still smaller ρ, approaching the scale of the van der Waals length $a_{\rm vdW} = 4.24 \times 10^2 a_0$, the quasi-2D DDI softens, no longer diverging as rapidly as $1/\rho^3$ (see Fig. 2 of Ref. [58]). In this limit, then, the interaction becomes dominated by the strong centrifugal repulsion of the molecules which, it will be recalled, possess relative angular momentum $m = 1$. Finally, at the smallest length scales, $\rho < a_{\rm vdW}$, the van der Waals interaction overwhelms everything, producing a potential barrier of height ≈ 10 μK peaking at $\rho \approx 0.007 a_d$ in Fig. 2 [63]. For still smaller values of ρ, there occurs exchange potentials and the possibility for sticking collisions [64, 65] or chemistry in reactive species. These processes are not dealt with explicitly here, but are represented by subjecting the wave functions to absorbing boundary conditions that also remove any other CIR [66].

Confinement has a significant effect on the formation and properties of this bound state. Note that the molecules are asymptotically in their ground states, whereby if they interact in free 3D space, the lowest adiabatic potential curve would be purely attractive; no such bound state would then exist. Moreover, being in the molecular ground states, there are no lower-energy open channels in which the CIFLs can decay, which circumstance greatly enhances its stability, see below.

The lifetime of the CIFL state is, therefore, governed by the tunneling rate through the potential barrier at $\rho \approx a_{\rm vdW}$, where the molecules are assumed to

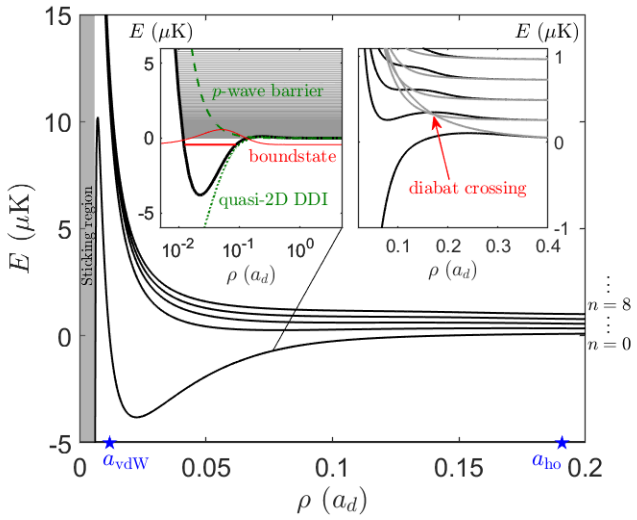

FIG. 2. The 5 lowest adiabats (solid black curves) between two z-confined $Na^{23}K^{40}$ molecules with $\omega_z = 2\pi \times 2.5$ kHz, subject to an applied electric field of $\mathcal{E} = 15$ kV/cm. The van der Waals and harmonic oscillator lengths are indicated by blue stars on the ρ-axis (labeled in plot), while the short-range sticking region is shaded in gray. The left inset is a log-linear plot of the DVR eigenenergies (horizontal solid lines) of the lowest adiabat (solid black curve), showing a CIFLs (red) with $E < 0$, apart from the quasi-continuum states (gray) with $E > 0$. The lowest adiabat comprises a quasi-2D DDI component (dotted green curve) and a p-wave barrier (dashed green curve). The right inset gives a zoomed in plot of the adiabats, overlayed with the diagonal entries of $U^{m=1}_{n',n}(\rho)$ as solid light gray curves, showing a crossing of the 2 lowest diabats.

be lost if they undergo this tunneling. Utilizing the Wentzel–Kramers–Brillouin (WKB) approximation, the tunneling probability is computed as:

$$p_{\rm WKB} = \exp\left(-2\int_{\tilde{\rho}_{\rm in}}^{\tilde{\rho}_{\rm out}} d\tilde{\rho}\sqrt{\tilde{U}_{\rm ad}(\rho) - \tilde{E}_{\rm CIFL}}\right), \quad (5)$$

where $\rho_{\rm in}$ and $\rho_{\rm out}$ indicate the inner and outer turning points of the potential barrier at CIFLs energy $E_{\rm CIFL}$ respectively. The inverse transmission rate through the short-range barrier then gives a semiclassical estimate of the lifetime

$$\tau_{\rm WKB}(E_{\rm CIFL}) \approx \left(\frac{v(E_0)}{2\Delta\rho_{E_{\rm CIFL}}} p_{\rm WKB}(E_{\rm CIFL})\right)^{-1}, \quad (6)$$

where

$$v(E_{\rm CIFL}) = \int_{\rho_{\rm out}}^{\rho_{\rm end}} d\rho |u_{\rm CIFL}(\rho)|^2 \sqrt{\frac{2}{\mu}[E_{\rm CIFL} - U_{\rm ad}(\rho)]}$$

is the mean kinetic velocity of the bound state, $u_{\rm CIFL}(\rho)$ is the radial wavefunction of the CIFLs and $\Delta\rho_E$ is the distance between classical turning points in the classically allowed part of the potential well at $E_{\rm CIFL}$. For NaK with its bound state depicted in Fig. 2, the WKB tunneling probability is around $p_{\rm WKB} \approx 5.8 \times 10^{-7}$, from which we estimate a lifetime of $\tau_{\rm WKB} \approx 29$ s. This predicted lifetime is about 3600 times longer than those observed for field-linked molecules in 3D [50].

Observing CIFLs. A CIFLs only emerges at a critical value of electric field $\mathcal{E} = \mathcal{E}^*$, large enough to induce a sufficiently deep potential well that supports a bound state. In experiments with bulk gaseous samples, the emergence of this bound state will be observed as a scattering resonance as the electric field is ramped across $\mathcal{E}^*$. To this end, we perform multichannel scattering calculations of two NaK molecules for a range of $\mathcal{E}$ values with $\omega_z = 2\pi \times 2.5$ kHz. Our calculations utilize an adaptive step-size version of the Johnson log-derivative propagator method [67], from which we quantify resonances in terms of the elastic integral cross section

$$\sigma = \frac{2\pi}{k^2}\sum_m \sum_{n',n} \left|T^m_{n',n}(k)\right|^2, \quad (7)$$

where $T^m_{n',n}(k)$ is the k-dependent T-matrix for partial wave m, connecting the n quantum numbers during a scattering event. Relevant to current ultracold molecule experiments, we consider a collision energy of 200 nK, which is smaller than $2\hbar\omega_z \approx 240$ nK, but larger than the DDI barrier (≈ 110 nK). This choice prevents the presence of shape resonances from the DDI barrier, while maintaining a single open scattering channel. Numerical propagation is performed with a short-range capture boundary condition [68] at $\rho_{\rm capture} = (8\pi\epsilon_0 C_6/d^2)^{1/3}$, the distance at which the DDI and van der Waals interaction become comparable [56]. We utilize up to the $n = 14$ harmonic oscillator state and $m = 9$ partial wave to converge the calculations.

Fixing $\omega_z = 2\pi \times 2.5$ kHz, we plot σ as a function of $\mathcal{E}$ in subplot (a) of Fig. 3, which shows a resonance in the cross section near $\mathcal{E}^* \approx 8$ kV/cm. We also plot the elastic scattering phase shift for the $m = 1$ partial wave $\delta_{\rm el}$ as a dashed red curve, which makes an excursion across $-\pi/2$ also around 8 kV/cm. By diagonalizing the Hamiltonian of $U_{\rm ad}(\rho)$ in its discrete variable representation (DVR) [69], we obtain the binding energy of the CIFLs that emerges around $\mathcal{E}^* \approx 9$ kV/cm, shown in subplot (b) of Fig. 3. We attribute the slight discrepancy between $\mathcal{E}^*$ from close-coupling and DVR calculations to the finite 200 nK collision energy that is outside the 2D threshold scattering regime. For comparison, we plot the cross section obtained in the single-mode approximation by setting $n' = n = 0$ in Eq. (3), but converged in partial waves. No CIFLs resonance is observed for this calculation, but only a monotonic increase of σ with $\mathcal{E}$ similar to the close-to-threshold $\sigma \sim a_d^2$ behavior in pure 2D [70] [see also subplot (b) of Fig. 4].

Alongside their control with electric fields, a CIFLs

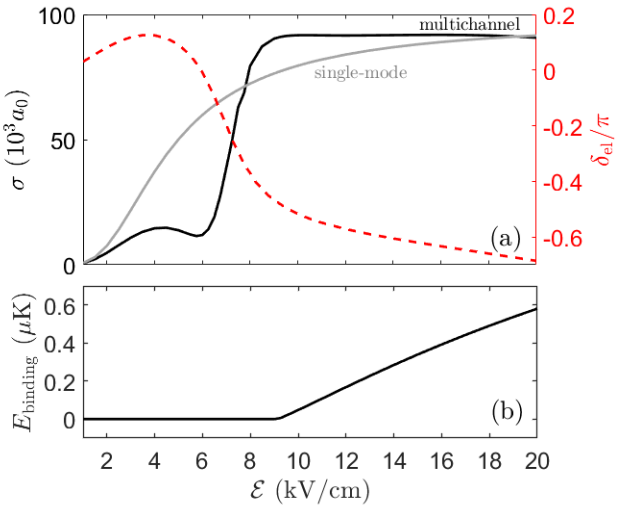

FIG. 3. Subplot (a) plots the integral cross section (solid black curve) and elastic scattering phase shift for the $m = 1$ partial wave (dashed red curve) as a function of $\mathcal{E}$, while subplot (b) plots the binding energy obtained from DVR calculations as a function of $\mathcal{E}$. The phase shift is seen to make an excursion across $-\pi/2$ as a bound state emerges, leading to a resonance of the elastic scattering cross section. We also plot σ vs $\mathcal{E}$ obtained from the single-mode approximation ($n' = n = 0$) as a light gray curve in subplot (a).

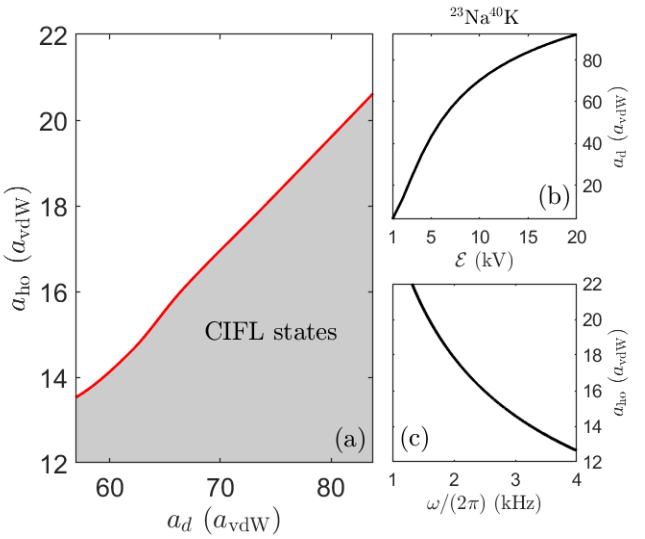

FIG. 4. (a) The range of $a_d/a_{\rm vdW}$ and $a_{\rm ho}/a_{\rm vdW}$ where the lowest adiabat supports a CIFLs is plotted as a gray region. (b) The effective dipole length a_d as a function of applied electric field $\mathcal{E}$ for ^{23}Na^{40}K. (c) The harmonic oscillator length $a_{\rm ho}$ as a function of trap frequency ω_z for ^{23}Na^{40}K.

is also tunable by means of the vertical trapping frequency. This tunability with confinement is illustrated in subplot (a) of Fig. 4, showing that the critical value $\mathcal{E}^*$ where a CIFLs emerges (solid red curve) changes as we vary ω_z. Each point in the region bounded below this solid red curve (gray region) contains an eigenstate with nonzero binding energy, derived from the DVR spectrum as in subplot (b) of Fig. 3. We present subplot (a) of Fig. 4 in terms of the adimensional lengths $a_d/a_{\rm vdW}$ and $a_{\rm ho}/a_{\rm vdW}$, both monotonic functions of $\mathcal{E}$ and ω_z respectively as shown in subplots (b) and (c) of the same figure for the case of ^{23}Na^{40}K. Subplot (a) is then interpretable in a molecule-agnostic fashion, in that the $\mathcal{E}$ and ω_z values necessary to observe a CIFLs resonance can be inferred for other molecules given their masses, rotational constants and van der Waals coefficients.

In summary, we have introduced a new set of confinement-induced field-linked states between ultracold polar molecules in the presence of a static electric field and 1D harmonic confinement. Supported in the lowest molecular adiabat, the propensity of these states to enter the short-range can be tuned via the electric field which changes the height of the inner p-wave barrier. This sensitivity to electric field makes them prime candidates for controlled studies of sticking dynamics and molecular chemistry. Varying both the applied field and confinement appropriately could also reduce the spatial extent of the CIFLs, opening opportunities for STIRAP of the molecules into their true tetramer groundstate. In addition, the presence of such a resonance will be critical in efforts to create pairing interactions between these fermionic species.

We comment that in the same setting discussed but with bosonic molecules, s-wave scattering is symmetry-allowed, removing the short-range p-wave barrier that prevents chemically reactive or sticking dynamics. A workaround to this shortcoming might be achieved by preparing the molecules in their relative $n = 1$ harmonic oscillator state, such that even symmetry of the molecular-pair wavefunction only permits scattering in odd partial waves. We leave further investigations of this to a future publication.

Acknowledgments. This material is based upon work supported by the National Science Foundation under Grant Number PHY 2317149. R.R.W.W. acknowledges partial support from the NSF through a grant for ITAMP at Harvard University.

[1] B. Yan, S. A. Moses, B. Gadway, J. P. Covey, K. R. A. Hazzard, A. M. Rey, D. S. Jin, and J. Ye, Nature **501**, 521 (2013).
[2] L. Reichsöllner, A. Schindewolf, T. Takekoshi, R. Grimm, and H.-C. Nägerl, Phys. Rev. Lett. **118**, 073201 (2017).
[3] J. Lin, J. He, M. Jin, G. Chen, and D. Wang, Phys. Rev. Lett. **128**, 223201 (2022).
[4] L. Christakis, J. S. Rosenberg, R. Raj, S. Chi, A. Morningstar, D. A. Huse, Z. Z. Yan, and W. S. Bakr, Nature **614**, 64 (2023).

[5] C. Miller, A. N. Carroll, J. Lin, H. Hirzler, H. Gao, H. Zhou, M. D. Lukin, and J. Ye, Two-axis twisting using floquet-engineered xyz spin models with polar molecules (2024), arXiv:2404.18913 [cond-mat.quant-gas].
[6] M. H. G. de Miranda, A. Chotia, B. Neyenhuis, D. Wang, G. Quéméner, S. Ospelkaus, J. L. Bohn, J. Ye, and D. S. Jin, Nature Physics **7**, 502 (2011).
[7] W. G. Tobias, K. Matsuda, J.-R. Li, C. Miller, A. N. Carroll, T. Bilitewski, A. M. Rey, and J. Ye, Science **375**, 1299 (2022), https://www.science.org/doi/pdf/10.1126/science.abn8525.
[8] J.-R. Li, K. Matsuda, C. Miller, A. N. Carroll, W. G. Tobias, J. S. Higgins, and J. Ye, Nature **614**, 70 (2023).
[9] A. N. Carroll, H. Hirzler, C. Miller, D. Wellnitz, S. R. Muleady, J. Lin, K. P. Zamarski, R. R. W. Wang, J. L. Bohn, A. M. Rey, and J. Ye, Observation of generalized t-j spin dynamics with tunable dipolar interactions (2024), arXiv:2404.18916 [cond-mat.quant-gas].
[10] I. Bloch, J. Dalibard, and W. Zwerger, Rev. Mod. Phys. **80**, 885 (2008).
[11] V. Dunjko, M. G. Moore, T. Bergeman, and M. Olshanii, in *Advances in Atomic, Molecular, and Optical Physics*, Advances In Atomic, Molecular, and Optical Physics, Vol. 60, edited by E. Arimondo, P. Berman, and C. Lin (Academic Press, 2011) pp. 461–510.
[12] M. Olshanii, Phys. Rev. Lett. **81**, 938 (1998).
[13] D. S. Petrov and G. V. Shlyapnikov, Phys. Rev. A **64**, 012706 (2001).
[14] T. Bergeman, M. G. Moore, and M. Olshanii, Phys. Rev. Lett. **91**, 163201 (2003).
[15] S. Saeidian, V. S. Melezhik, and P. Schmelcher, Phys. Rev. A **77**, 042721 (2008).
[16] P. Giannakeas, V. S. Melezhik, and P. Schmelcher, Phys. Rev. Lett. **111**, 183201 (2013).
[17] T. Shi and S. Yi, Phys. Rev. A **90**, 042710 (2014).
[18] S. Sala and A. Saenz, Phys. Rev. A **94**, 022713 (2016).
[19] E. Haller, M. J. Mark, R. Hart, J. G. Danzl, L. Reichsöllner, V. Melezhik, P. Schmelcher, and H.-C. Nägerl, Phys. Rev. Lett. **104**, 153203 (2010).
[20] Y. K. Lee, H. Lin, and W. Ketterle, Phys. Rev. Lett. **131**, 213001 (2023).
[21] D. Capecchi, C. Cantillano, M. J. Mark, F. Meinert, A. Schindewolf, M. Landini, A. Saenz, F. Revuelta, and H.-C. Nägerl, Phys. Rev. Lett. **131**, 213002 (2023).
[22] M. Pinkas, O. Katz, J. Wengrowicz, N. Akerman, and R. Ozeri, Nature Physics **19**, 1573 (2023).
[23] H. P. Büchler, E. Demler, M. Lukin, A. Micheli, N. Prokof'ev, G. Pupillo, and P. Zoller, Phys. Rev. Lett. **98**, 060404 (2007).
[24] A. V. Gorshkov, S. R. Manmana, G. Chen, J. Ye, E. Demler, M. D. Lukin, and A. M. Rey, Phys. Rev. Lett. **107**, 115301 (2011).
[25] A. V. Gorshkov, S. R. Manmana, G. Chen, E. Demler, M. D. Lukin, and A. M. Rey, Phys. Rev. A **84**, 033619 (2011).
[26] A. Kruckenhauser, L. M. Sieberer, L. De Marco, J.-R. Li, K. Matsuda, W. G. Tobias, G. Valtolina, J. Ye, A. M. Rey, M. A. Baranov, and P. Zoller, Phys. Rev. A **102**, 023320 (2020).
[27] A. V. Avdeenkov and J. L. Bohn, Phys. Rev. A **66**, 052718 (2002).
[28] A. V. Avdeenkov and J. L. Bohn, Phys. Rev. Lett. **90**, 043006 (2003).
[29] A. V. Avdeenkov, D. C. E. Bortolotti, and J. L. Bohn, Phys. Rev. A **69**, 012710 (2004).
[30] A. V. Avdeenkov and J. L. Bohn, Phys. Rev. A **71**, 022706 (2005).
[31] A. V. Avdeenkov, M. Kajita, and J. L. Bohn, Phys. Rev. A **73**, 022707 (2006).
[32] G. Quéméner and J. L. Bohn, Phys. Rev. A **93**, 012704 (2016).
[33] M. L. González-Martínez, J. L. Bohn, and G. Quéméner, Phys. Rev. A **96**, 032718 (2017).
[34] L. Lassablière and G. Quéméner, Phys. Rev. A **106**, 033311 (2022).
[35] A. V. Avdeenkov, Phys. Rev. A **86**, 022707 (2012).
[36] L. Lassablière and G. Quéméner, Phys. Rev. Lett. **121**, 163402 (2018).
[37] T. Karman and J. M. Hutson, Phys. Rev. Lett. **121**, 163401 (2018).
[38] T. Karman, Phys. Rev. A **101**, 042702 (2020).
[39] K. Matsuda, L. D. Marco, J.-R. Li, W. G. Tobias, G. Valtolina, G. Quéméner, and J. Ye, Science **370**, 1324 (2020).
[40] J.-R. Li, W. G. Tobias, K. Matsuda, C. Miller, G. Valtolina, L. De Marco, R. R. Wang, L. Lassablière, G. Quéméner, J. L. Bohn, *et al.*, Nature Physics **17**, 1144 (2021).
[41] B. Mukherjee and J. M. Hutson, Phys. Rev. Res. **6**, 013145 (2024).
[42] L. Anderegg, S. Burchesky, Y. Bao, S. S. Yu, T. Karman, E. Chae, K.-K. Ni, W. Ketterle, and J. M. Doyle, Science **373**, 779 (2021).
[43] Z. Z. Yan, J. W. Park, Y. Ni, H. Loh, S. Will, T. Karman, and M. Zwierlein, Phys. Rev. Lett. **125**, 063401 (2020).
[44] G. Valtolina, K. Matsuda, W. G. Tobias, J.-R. Li, L. De Marco, and J. Ye, Nature **588**, 239 (2020).
[45] A. Schindewolf, R. Bause, X.-Y. Chen, M. Duda, T. Karman, I. Bloch, and X.-Y. Luo, Nature **607**, 677 (2022).
[46] J. Lin, G. Chen, M. Jin, Z. Shi, F. Deng, W. Zhang, G. Quéméner, T. Shi, S. Yi, and D. Wang, Phys. Rev. X **13**, 031032 (2023).
[47] N. Bigagli, C. Warner, W. Yuan, S. Zhang, I. Stevenson, T. Karman, and S. Will, Nature Physics **19**, 1579 (2023).
[48] N. Bigagli, W. Yuan, S. Zhang, B. Bulatovic, T. Karman, I. Stevenson, and S. Will, Nature 10.1038/s41586-024-07492-z (2024).
[49] X.-Y. Chen, A. Schindewolf, S. Eppelt, R. Bause, M. Duda, S. Biswas, T. Karman, T. Hilker, I. Bloch, and X.-Y. Luo, Nature **614**, 59 (2023).
[50] X.-Y. Chen, S. Biswas, S. Eppelt, A. Schindewolf, F. Deng, T. Shi, S. Yi, T. A. Hilker, I. Bloch, and X.-Y. Luo, Nature **626**, 283 (2024).
[51] G. Quéméner, J. L. Bohn, and J. F. E. Croft, Phys. Rev. Lett. **131**, 043402 (2023).
[52] M. A. Baranov, M. S. Mar'enko, V. S. Rychkov, and G. V. Shlyapnikov, Phys. Rev. A **66**, 013606 (2002).
[53] M. A. Baranov, L. Dobrek, and M. Lewenstein, Phys. Rev. Lett. **92**, 250403 (2004).
[54] F. Deng, X.-Y. Chen, X.-Y. Luo, W. Zhang, S. Yi, and T. Shi, Phys. Rev. Lett. **130**, 183001 (2023).
[55] M. Lepers, R. Vexiau, M. Aymar, N. Bouloufa-Maafa, and O. Dulieu, Phys. Rev. A **88**, 032709 (2013).
[56] A. Micheli, G. Pupillo, H. P. Büchler, and P. Zoller, Phys. Rev. A **76**, 043604 (2007).
[57] Further details of this quasi-2D interaction potential between bialkali polar molecules can be found in Ref. [56].
[58] C. Ticknor, Phys. Rev. A **81**, 042708 (2010).

[59] J. L. Bohn and D. S. Jin, Phys. Rev. A **89**, 022702 (2014).

[60] This bound state is part of the spectrum obtained by placing the molecules in a box with boundaries from $\rho = 0.005a_d$ to $\rho = 10a_d$, and diagonalizing the single-channel Hamiltonian with $U_{\rm ad}(\rho)$ in the discrete variable representation [69].

[61] G. Quéméner and J. L. Bohn, Phys. Rev. A **83**, 012705 (2011).

[62] B. Zhu, G. Quéméner, A. M. Rey, and M. J. Holland, Phys. Rev. A **88**, 063405 (2013).

[63] At distances of $\rho = 0.5a_{\rm vdW} \approx 210a_0$ and larger, the largest absolute adiabatic van der Waals energy from diagonalizing $\int dz\varphi_{n'}(z)V_{\rm vdW}(\rho,z)\varphi_n(z)$ is more than 10^3 times smaller than the splitting of the lowest two dressed rotational states for the lowest field value considered ($\mathcal{E} = 1$ kV/cm). This ratio assures the validity of the polarized dipole approximation in Eq. (2b) in the region of the potential well supporting a CIFLs.

[64] J. F. E. Croft and J. L. Bohn, Phys. Rev. A **89**, 012714 (2014).

[65] R. Bause, A. Christianen, A. Schindewolf, I. Bloch, and X.-Y. Luo, The Journal of Physical Chemistry A **127**, 729 (2023).

[66] Z. Idziaszek, K. Jachymski, and P. S. Julienne, New Journal of Physics **17**, 035007 (2015).

[67] B. Johnson, Journal of Computational Physics **13**, 445 (1973).

[68] G. Wang and G. Quéméner, New Journal of Physics **17**, 035015 (2015).

[69] D. T. Colbert and W. H. Miller, The Journal of Chemical Physics **96**, 1982 (1992), https://pubs.aip.org/aip/jcp/article-pdf/96/3/1982/18997949/1982_1_online.pdf.

[70] C. Ticknor, Phys. Rev. A **80**, 052702 (2009).

[71] A. Simoni, S. Srinivasan, J.-M. Launay, K. Jachymski, Z. Idziaszek, and P. S. Julienne, New Journal of Physics **17**, 013020 (2015).